Deep Latent State Space Models for Time-Series Generation

Linqi Zhou [1] **Michael Poli** [1] **Winnie Xu** [2] **Stefano Massaroli** [3] **Stefano Ermon** [1]

Abstract

Methods based on ordinary differential equations (ODEs) are widely used to build generative models of time-series. In addition to high computational overhead due to explicitly computing hidden states recurrence, existing ODE–based models fall short in learning sequence data with sharp transitions – common in many real-world systems – due to numerical challenges during optimization. In this work, we propose LS4, a generative model for sequences with latent variables evolving according to a state space ODE to increase modeling capacity. Inspired by recent deep state space models (S4), we achieve speedups by leveraging a convolutional representation of LS4 which bypasses the explicit evaluation of hidden states. We show that LS4 significantly outperforms previous continuous-time generative models in terms of marginal distribution, classification, and prediction scores on real-world datasets in the Monash Forecasting Repository, and is capable of modeling highly stochastic data with sharp temporal transitions. LS4 sets state–of–the–art for continuous–time latent generative models, with significant improvement of mean squared error and tighter variational lower bounds on irregularly–sampled datasets, while also being $\times 100$ faster than other baselines on long sequences.

1. Introduction

Time series are a ubiquitous data modality, and find extensive application in weather (Hersbach et al., 2020) engineering disciplines, biology (Peng et al., 1995), and finance (Poli et al., 2019). The main existing approaches for deep generative learning of temporal data can be broadly categorized into autoregressive (Oord et al., 2016), latent autoencoder models (Chen et al., 2018; Yildiz et al., 2019; Rubanova et al., 2019), normalizing flows (de Bézenac et al., 2020), generative adversarial (Yoon et al., 2019; Yu et al., 2022; Brooks et al., 2022), and diffusion (Rasul et al., 2021). Among these, continuous-time methods (often based on underlying ODEs) are the preferred approach for irregularly-sampled sequences as they can predict at arbitrary time steps and can handle sequences of varying lengths. Unfortunately, existing ODE–based methods (Rubanova et al., 2019; Yildiz et al., 2019) often fall short in learning models for real-world data (*e.g.*, temperature and rain data that follow very sharp transition dynamics) due to their limited expressivity and numerical instabilities during backward gradient computation (Hochreiter, 1998; Niesen & Hall, 2004; Zhuang et al., 2020).

A natural way to increase the flexibility of ODE-based models is to increase the dimensionality of their (deterministic) hidden states. State–of–the–art methods explicitly compute hidden states by unrolling the underlying recurrence over time (each time step parametrized by a neural network), incurring in polynomial computational costs which prevent scaling to longer sequences.

An alternative approach to increasing modeling capacity is to incorporate *stochastic* latent variables into the model, a highly successful strategy in generative modeling (Kingma & Welling, 2013; Chung et al., 2015; Song et al., 2020; Ho et al., 2020). However, reference models like latent neural ODE models (Rubanova et al., 2019) inject stochasticity only at the initial condition of the system. In contrast, we introduce LS4, a latent generative model where the sequence of latent variables is represented as the solution of linear state space equations (Chen, 1984). Unrolling the recurrence equation shows an autoregressive dependence in the sequence of latent variables, the joint of which is highly expressive in representing time series distributions. The high dimensional structure of the latent space, being equivalent to that of the input sequence, allows LS4 to learn expressive latent representations and fit the distribution of sequences produced by a *family* of dynamical systems, a common setting resulting from non–stationarity. We further show how LS4 can learn the dynamics of *stiff* (Shampine & Thompson, 2007) dynamical systems where previous methods fail to do so. Inspired by recent works on deep state space models, or stacks of linear state spaces and non-linearities (Gu

[1]Stanford University [2]University of Toronto [3]MILA. Correspondence to: Linqi Zhou <linqizhou@stanford.edu>, Michael Poli <poli@stanford.edu>.

Proceedings of the 40^{th} International Conference on Machine Learning, Honolulu, Hawaii, USA. PMLR 202, 2023.

et al., 2020; 2021), we leverage a convolutional kernel representation to solve the recurrence, bypassing any explicit computations of hidden states via the recurrence equation, which ensures log–linear scaling in both the hidden state space dimensionality as well as sequence length.

We validate our method across a variety of time series datasets, benchmarking LS4 against an extensive set of baselines. We propose a set of 3 metrics to measure the quality of generated time series samples and show that LS4 performs significantly better than baselines on datasets with stiff transitions and obtains on average 30% lower MSE scores and ELBO. On sequences with $\approx 20K$ lengths, our model trains $\times 100$ faster than the baseline methods.

2. Related Work

Rapid progress on deep generative modeling of natural language and images has consolidated diffusion (Ho et al., 2020; Song et al., 2020; Song & Ermon, 2019; Sohl-Dickstein et al., 2015) and autoregressive techniques (Brown et al., 2020) as the state–of–the–art. Although various approaches have been proposed for generative modeling of time series and dynamical systems, consensus on the advantages and disadvantages of each method has yet to emerge.

Deep generative modeling of sequences. All the major paradigms for deep generative modeling have seen applications to time series and sequences. Prior works for time-series generation have adopted VAE-, Flow-, and GAN-based approaches (Chung et al., 2015; Deng et al., 2020; Yu et al., 2017; Yoon et al., 2019) which utilize recurrent architectures to keep track of internal states. For continuous–time data, other works combine Gaussian processes (Fortuin et al., 2020) or ODEs (Yildiz et al., 2019; Rubanova et al., 2019) into their probabilistic frameworks and show promising results for time-series extrapolation and generation. Other works on time-series have adopted diffusion-based frameworks (Tashiro et al., 2021), but similar to the methods requiring recurrent computations, these methods suffer from prolonged generation time. Among these methods, most relevant to our work are latent continuous–time autoencoder models proposed by Chen et al. (2018); Yildiz et al. (2019); Rubanova et al. (2019), where a neural differential equation encoder is used to parameterize as distribution of initial conditions for the decoder. Massaroli et al. (2021) proposes a variant that parallelizes computation in time by casting solving the ODE as a root finding problem. Beyond latent models, other continuous–time approaches are given in Kidger et al. (2020), which develops a GAN formulation using SDEs.

State space models. *State space models* (SSMs) are at the foundation of dynamical system theory (Chen, 1984) and signal processing (Oppenheim, 1999), and have also been adapted to deep generative modeling. Chung et al. (2015); Bayer & Osendorfer (2014) propose VAE variants of discrete–time RNNs, generalized later by (Franceschi et al., 2020), among others. However, these models all unroll the recurrence equation and are thus challenging to scale to longer sequences.

Our work is inspired by recent advances in deep architectures built as stacks of linear SSMs, notably S4 (Gu et al., 2021; 2020). The HiPPO-initialized and deeply stacked linear SSMs have shown promising results for modeling long sequences with unprecedented efficiency, and they have shown remarkable modeling capacity for capturing long-range dependencies across large time scale. Similar to S4, our generative model leverages the convolutional representation of SSMs during training and inference, thus bypassing the need to materialize the hidden state of each recurrence. This allows us to speed up training and inference by a large margin compared to prior generative methods. More importantly, we augment the deep SSMs to model sequential latent variables, which increase the capacity to capture more complex temporal dynamics (*e.g.* stiff transitions) and achieve better generation results.

3. Preliminaries

We briefly introduce relevant details of continuous-time SSMs and their different representations. Then we introduce preliminaries of generative models for sequences.

3.1. State Space Models (SSM)

A *single-input single-output (SISO)* linear state space model is defined by the following differential equation

$$\begin{aligned} \frac{d}{dt}\boldsymbol{h}_t &= \boldsymbol{A}\boldsymbol{h}_t + \boldsymbol{B}x_t \\ y_t &= \boldsymbol{C}\boldsymbol{h}_t + \boldsymbol{D}x_t \end{aligned} \tag{1}$$

with scalar *input* $x_t \in \mathbb{R}$, *state* $\boldsymbol{h}_t \in \mathbb{R}^N$ and scalar *output* $y_t \in \mathbb{R}$. The system is fully characterized by the matrices $\boldsymbol{A} \in \mathbb{R}^{N\times N}, \boldsymbol{B} \in \mathbb{R}^{N\times 1}, \boldsymbol{C} \in \mathbb{R}^{1\times N}, \boldsymbol{D} \in \mathbb{R}^{1\times 1}$. Let $x, y \in \mathcal{C}([a, b], \mathbb{R})$ be absolutely continuous real signals on time interval $[a, b]$. Given an initial condition $\boldsymbol{h}_0 \in \mathbb{R}^N$ the SSM (1) realizes a mapping $x \mapsto y$.

SSMs are a common tool for processing continuous input signals. We consider *single input single output* (SISO) SSMs, noting that input sequences with more than a single channel can be processed by applying multiple SISO SSMs in parallel, similarly to regular convolutional layers. We use such SSMs as building blocks to map each input dimension to each output dimension in our generative model.

Discrete recurrent representation. In practice, continuous input signals are often sampled at time interval Δ and the

sampled sequence is represented by $x = (x_{t_0}, x_{t_1}, \ldots, x_{t_L})$ where $t_{k+1} = t_k + \Delta$. The discretized SSM follows the recurrence

$$\begin{aligned} \boldsymbol{h}_{t_{k+1}} &= \bar{\boldsymbol{A}}\boldsymbol{h}_{t_k} + \bar{\boldsymbol{B}}x_{t_k} \\ y_{t_k} &= \boldsymbol{C}\boldsymbol{h}_{t_k} + \boldsymbol{D}x_{t_k} \end{aligned} \tag{2}$$

where $\bar{\boldsymbol{A}} = e^{\boldsymbol{A}\Delta}$, $\bar{\boldsymbol{B}} = \boldsymbol{A}^{-1}(e^{\boldsymbol{A}\Delta} - I)\boldsymbol{B}$ with the assumption that signals are constant during the sampling interval.

Among many approaches to efficiently computing $e^{\boldsymbol{A}\Delta}$, Gu et al. (2021) use a bilinear transform to estimate $e^{\boldsymbol{A}\Delta} \approx (I - \frac{1}{2}\boldsymbol{A}\Delta)^{-1}(I + \frac{1}{2}\boldsymbol{A}\Delta)$.

This recurrence equation can be used to iteratively solve for the next hidden state $h_{t_{k+1}}$, allowing the states to be calculated like an RNN or a Neural ODE (Chen et al., 2018; Massaroli et al., 2020).

Convolutional representation. Recurrent representations of SSM are not practical in training because explicit calculation of hidden states for every time step requires $\mathcal{O}(N^2L)$ in time and $\mathcal{O}(NL)$ in space for a sequence of length L[1]. This materialization of hidden states significantly restricts RNN-based methods in scaling to long sequences. To efficiently train an SSM, the recurrence equation can be fully unrolled, assuming zero initial hidden states, as

$$\begin{aligned} \boldsymbol{h}_{t_0} &= \bar{\boldsymbol{B}}x_{t_0} & \boldsymbol{h}_{t_1} &= \bar{\boldsymbol{A}}\bar{\boldsymbol{B}}x_{t_1} + \bar{\boldsymbol{B}}x_{t_0} \\ y_{t_0} &= \boldsymbol{C}\bar{\boldsymbol{B}}x_{t_0} & y_{t_1} &= \boldsymbol{C}\bar{\boldsymbol{A}}\bar{\boldsymbol{B}}x_{t_1} + \boldsymbol{C}\bar{\boldsymbol{B}}x_{t_0} \end{aligned}$$

$$\begin{aligned} \boldsymbol{h}_{t_2} &= \bar{\boldsymbol{A}}^2\bar{\boldsymbol{B}}x_{t_2} + \bar{\boldsymbol{A}}\bar{\boldsymbol{B}}x_{t_1} + \bar{\boldsymbol{B}}x_{t_0} & \ldots \\ y_{t_2} &= \boldsymbol{C}\bar{\boldsymbol{A}}^2\bar{\boldsymbol{B}}x_{t_2} + \boldsymbol{C}\bar{\boldsymbol{A}}\bar{\boldsymbol{B}}x_{t_1} + \boldsymbol{C}\bar{\boldsymbol{B}}x_{t_0} & \ldots \end{aligned}$$

and more generally as,

$$y_{t_k} = \boldsymbol{C}\bar{\boldsymbol{A}}^k\bar{\boldsymbol{B}}x_{t_k} + \boldsymbol{C}\bar{\boldsymbol{A}}^{k-1}\bar{\boldsymbol{B}}x_{k-1} + \cdots + \boldsymbol{C}\bar{\boldsymbol{B}}x_{t_0}$$

For an input sequence $x = (x_{t_0}, x_{t_1}, \ldots, x_{t_L})$, one can observe that the output sequence $y = (y_{t_0}, y_{t_1}, \ldots, y_{t_L})$ can be computed using a convolution with a skip connection

$$\begin{aligned} y &= \boldsymbol{C}\boldsymbol{K} * x + \boldsymbol{D}x, \\ &\text{where } \boldsymbol{K} = (\bar{\boldsymbol{B}}, \bar{\boldsymbol{A}}\bar{\boldsymbol{B}}, \ldots, \bar{\boldsymbol{A}}^{L-1}\bar{\boldsymbol{B}}, \bar{\boldsymbol{A}}^{L}\bar{\boldsymbol{B}}) \end{aligned} \tag{3}$$

This is the well-known connection between SSM and convolution (Oppenheim & Schafer, 1975; Chen, 1984; Chilkuri & Eliasmith, 2021; Romero et al., 2021; Gu et al., 2020; 2021; 2022)

and it can be computed very efficiently with a Fast Fourier Transform (FFT), which scales better than explicit matrix multiplication at each step.

[1]Further explanations in Appendix A.1

3.2. Variational Autoencoder (VAE)

VAEs (Kingma & Welling, 2013; Burda et al., 2015) are a highly successful paradigm in learning latent representations of high dimensional data and is remarkably capable at modeling complex distributions. A VAE introduces a joint probability distribution between a latent variable $\boldsymbol{z}$ and an observed random variable $\boldsymbol{x}$ of the form

$$p_\theta(\boldsymbol{x}, \boldsymbol{z}) = p_\theta(\boldsymbol{x} \mid \boldsymbol{z})p(\boldsymbol{z})$$

where θ represents learnable parameters.

The prior $p(\boldsymbol{z})$ over the latent is usually chosen as a standard Gaussian distribution, and the conditional distribution $p_\theta(\boldsymbol{x} \mid \boldsymbol{z})$ is defined through a flexible non-linear mapping (such as a neural network) taking $\boldsymbol{z}$ as input.

Such highly flexible non-linear mappings often lead to an intractable posterior $p_\theta(\boldsymbol{z} \mid \boldsymbol{x})$. Therefore, an inference model with parameters ϕ parametrizing $q_\phi(\boldsymbol{z} \mid \boldsymbol{x})$ is introduced as an approximation which allows learning through a variational lower bound of the marginal likelihood:

$$\begin{aligned} \log p_\theta(\boldsymbol{x}) \geq &-D_{\mathrm{KL}}(q_\phi(\boldsymbol{z} \mid \boldsymbol{x}) \| p(\boldsymbol{z})) \\ &+ \mathbb{E}_{q_\phi(\boldsymbol{z}|\boldsymbol{x})}\left[\log p_\theta(\boldsymbol{x} \mid \boldsymbol{z})\right] \end{aligned} \tag{4}$$

where $D_{\mathrm{KL}}(\cdot\|\cdot)$ is the Kullback-Leibler divergence between two distributions.

VAE for sequences. Sequence data can be modeled in many different ways since the latent space can be chosen to encode information at different levels of granularity, *i.e.* $\boldsymbol{z}$ can be a single variable encoding entire trajectories or a sequence of variables of the same length as the trajectories. We focus on the latter.

Given observed sequence variables $\boldsymbol{x}_{\leq T}$ up to time T discretized into sequence $(\boldsymbol{x}_{t_0}, \ldots, \boldsymbol{x}_{t_{L-1}})$ of length L where $t_{L-1} = T$, a sequence VAE model with parameters θ, λ, ϕ learns a generative and inference distribution

$$p_{\theta,\lambda}(\boldsymbol{x}_{\leq t_{L-1}}, \boldsymbol{z}_{\leq t_{L-1}}) = \prod_{i=0}^{L-1} p_\theta(\boldsymbol{x}_{t_i} \mid \boldsymbol{x}_{<t_i}, \boldsymbol{z}_{\leq t_i}) p_\lambda(\boldsymbol{z}_t \mid \boldsymbol{z}_{<t_i})$$

$$q_\phi(\boldsymbol{z}_{\leq t_{L-1}} \mid \boldsymbol{x}_{\leq t_{L-1}}) = \prod_{i=0}^{L-1} q_\phi(\boldsymbol{z}_{t_i} \mid \boldsymbol{x}_{\leq t_i})$$

where $\boldsymbol{z}_{\leq t_{L-1}} = (\boldsymbol{z}_{t_0}, \ldots, \boldsymbol{z}_{t_{L-1}})$ is the corresponding latent variable sequence. The approximate posterior q_ϕ is explicitly factorized as a product of marginals due to efficiency reasons we shall discuss in the next section. Given this form of factorization, the variational lowerbound has been considered for discrete sequence data (Chung et al., 2015) by minimizing the objective

$$\begin{aligned} \mathbb{E}_{q_\phi(\boldsymbol{z}_{\leq t_{L-1}} | \boldsymbol{x}_{\leq t_{L-1}})}\Big[\sum_{i=0}^{L-1} &D_{\mathrm{KL}}(q_\phi(\boldsymbol{z}_{t_i} \mid \boldsymbol{x}_{\leq t_i}) \| p_\lambda(\boldsymbol{z}_i \mid \boldsymbol{z}_{<t_i})) \\ &- \log p_\theta(\boldsymbol{x}_{t_i} \mid \boldsymbol{x}_{<t_i} \boldsymbol{z}_{\leq t_i}) \Big] \end{aligned} \tag{5}$$

Our model also trains by this objective. After training, the generative model can then sample z_t from the prior p_λ autoregressively and given the sampled z_t, each x_t can be sampled autoregressively using $p_\theta(\boldsymbol{x}_{t_i} \mid \boldsymbol{x}_{<t_i} \boldsymbol{z}_{\leq t_i})$.

4. Method

In this section, we introduce *Latent S4* (LS4), a latent variable generative model parameterized using SSMs. We show how SSMs can parametrize the generative distribution $p_\theta(\boldsymbol{x}_{\leq T}|\boldsymbol{z}_{\leq T})p_\lambda(\boldsymbol{z}_{\leq T})$, the prior distribution $p_\lambda(\boldsymbol{z}_{\leq T})$ and the inference distribution $q_\phi(\boldsymbol{z}_{\leq T} \mid \boldsymbol{x}_{\leq T})$ effectively. For the purpose of exposition, we can assume z_t, x_t are scalars at any time step t. Their generalization to arbitrary dimensions is discussed in Section 4.4.

We first define a structured state space model with two input streams and use this as a building block for our generative model. It is an SSM of the form

$$\begin{aligned} \frac{d}{dt}\boldsymbol{h}_t &= \boldsymbol{A}\boldsymbol{h}_t + \boldsymbol{B}x_t + \boldsymbol{E}z_t \\ y_t &= \boldsymbol{C}\boldsymbol{h}_t + \boldsymbol{D}x_t + \boldsymbol{F}z_t \end{aligned}$$

where $x, y, z \in \mathcal{C}([0,T], \mathbb{R})$ are continuous real signals on time interval $[0,T]$. We denote $H(x, z, \boldsymbol{A}, \boldsymbol{B}, \boldsymbol{E}, \boldsymbol{h}_0, t) = H_\beta(x, z, \boldsymbol{h}_0, t)$, where β denotes trainable parameters $\boldsymbol{A}, \boldsymbol{B}, \boldsymbol{E}$, as the deterministic function mapping from signals x, z to $\boldsymbol{h}_t$, the state at time t, given initial state $\boldsymbol{h}_0$ at time 0. The above SSM can be compactly represented by

$$y_t = \boldsymbol{C}H_\beta(x, z, \boldsymbol{h}_0, t) + \boldsymbol{D}x_t + \boldsymbol{F}z_t \tag{6}$$

When the continuous-time input signals are discretized into discrete-time sequences $(x_{t_0}, \ldots, x_{t_{L-1}})$ and $(z_{t_0}, \ldots, z_{t_L})$, the corresponding hidden state at time t_k has a convolutional view (assuming $\boldsymbol{D} = \boldsymbol{F} = \boldsymbol{0}$ for simplicity)

$$\begin{aligned} y_{t_k} &= \boldsymbol{C}\boldsymbol{K}_{t_k} * x_{t_k} + \boldsymbol{C}\hat{\boldsymbol{K}}_{t_k} * z_{t_k}, \\ &\text{where } \boldsymbol{K}_{t_k} = \bar{\boldsymbol{A}}^k \bar{\boldsymbol{B}}, \ \hat{\boldsymbol{K}}_{t_k} = \bar{\boldsymbol{A}}^k \bar{\boldsymbol{E}} \end{aligned}$$

which can be evaluated efficiently using FFT. Additionally, $\boldsymbol{A}$ is HiPPO-initialized (Gu et al., 2021) for all such SSM blocks.

4.1. Latent Space as Structured State Space

The goal of the prior model is to realize a sequence of random variables $(z_{t_0}, z_{t_1}, \ldots, z_{t_L})$, which the prior distribution $p_\lambda(z_{\leq t_L})$ models autoregressively. Suppose $(z_{t_0}, z_{t_1}, \ldots, z_{t_n})$ is a sequence of latent variables up to time t_n, we define the prior distribution of z_{t_n} autoregressively as

$$p_\lambda(z_{t_n} \mid z_{<t_n}) = \mathcal{N}(\mu_{z,n}(z_{<t_n}, \lambda), \sigma^2_{z,n}(z_{<t_n}, \lambda)) \tag{7}$$

where the mean $\mu_{z,n}$ and standard deviation $\sigma_{z,n}$ are deterministic functions of previously generated $z_{<t_n}$ parameterized by λ. To parameterize the above distribution, we first define an intermediate building block, a stack of which will produce the wanted distribution.

LS4 prior block. The forward pass through our SSM is a two–step procedure: first, we consider the latent dynamics of z on $[t_0, t_{n-1}]$ where we simply leverage Equation 6 to define the hidden states to follow $H_{\beta_1}(0, z, 0, t)$. Second, on $(t_{n-1}, t_n]$, since no additional z is available in this interval, we ignore additional input signals in the ODE and only include the last given latent, *i.e.* $z_{t_{n-1}}$, as an auxiliary signal for the outputs, which can be compactly denoted, with a final GELU non-linearity (which is the default in Gu et al. (2021)), as

$$\begin{aligned} y_{z,n} = \text{GELU}(&\boldsymbol{F}_{y_z} z_{t_{n-1}} \\ &+ \boldsymbol{C}_{y_z} H_{\beta_1}(0, 0, \underbrace{H_{\beta_2}(0, z_{[t_0,t_{n-1}]}, h_{t_{n-1}}, \boldsymbol{0}, t_{n-1})}_{\boldsymbol{h}_{t_{n-1}}}, t_n)) \end{aligned} \tag{8}$$

Output $y_{z,n}$ has the same dimensionality as each z_t and is a function of all $z_{<t_n}$ and we will use it to build towards modeling the distribution of z_{t_n}. We call the above equation *LS4 prior layer* and we define below our *LS4 prior block*, which is built upon a ResNet structure with a skip connection, denoted as

$$\text{LS4}_{\text{prior}}(z_{[t_0,t_{n-1}]}, \psi) = \text{LN}(\boldsymbol{G}_{y_z} y_{z,n} + b_{y_z}) + z_{t_{n-1}} \tag{9}$$

where LN denotes LayerNorm and ψ denotes the union of parameters $\beta_i, \boldsymbol{C}_{y_z}, \boldsymbol{F}_{y_z}, \boldsymbol{G}_{y_z}, b_{y_z}$. The subscripts to these parameters indicate that they are specific to this prior block and are not shared across blocks. We define the final parameters $\mu_{z,n}$ and $\sigma_{z,n}$ for the conditional distribution in the autoregressive model as the result of a stack of *LS4 prior blocks*. Specifically, the input z_t's are input into a stack of B blocks and at the final layer two separate blocks branch out to separately parameterize $\mu_{z,n}$ and $\sigma_{z,n}$. During generation, as an initial condition, $z_{t_0} \sim \mathcal{N}(\mu_{z,0}, \sigma^2_{z,0})$ where $\mu_{z,0}, \sigma_{z,0}$ are learnable parameters, and subsequent latent variables are generated autoregressively. We specify our architecture in Appendix C and use λ to denote the union of all trainable parameters.

4.2. Generative Model

Given the latent variables, we now specify a decoder that represents the distribution $p_\theta(x_{\leq t_L}|z_{\leq t_L})$. Suppose $z_{\leq t_L}$ is a latent path generated via the latent state space model, the output path $x_{\leq t_L}$ also follows the state space formulation. Assuming we have generated $(x_{t_0}, \ldots, x_{t_{n-1}})$ and $(z_{t_0}, \ldots, z_{t_n})$, the conditional distribution of x_{t_n} is parametrized as

$$p_\theta(x_{t_n}|x_{<t_n}, z_{\leq t_n}) = \mathcal{N}(\mu_{x,n}(x_{<t_n}, z_{\leq t_n}, \theta), \sigma^2_x) \tag{10}$$

where σ_x is a pre-defined observation standard deviation and $\mu_{x,n}$ is a deterministic function of $z_{\leq t_n}$ and $x_{<x_n}$.

LS4 generative block. Different from the prior block, both observation and latent sequences are input into our model, and we define intermediate outputs $g_{x,n}$ and $g_{z,n}$ as

$$\begin{aligned} h_{t_n} =& H_{\beta_3}(0, z_{t_{n-1}}, H_{\beta_4}(x_{[t_0,t_{n-1}]}, z_{[t_0,t_{n-1}]}, \mathbf{0}, t_{n-1}), t_n) \\ g_{x,n} =& \text{GELU}(\boldsymbol{C}_{g_x} h_{t_n} + \boldsymbol{D}_{g_x} x_{t_{n-1}} + \boldsymbol{F}_{g_x} z_{t_n}) \\ g_{z,n} =& \text{GELU}(\boldsymbol{C}_{g_z} h_{t_n} + \boldsymbol{D}_{g_z} x_{t_{n-1}} + \boldsymbol{F}_{g_z} z_{t_n}) \end{aligned} \tag{11}$$

which are used to build a *LS4 generative block* defined as

$$\begin{aligned} \hat{g}_{x,n} &= \text{LN}(\boldsymbol{G}_{g_x} g_{x,n} + b_{g_x}) + x_{t_{n-1}} \\ \hat{g}_{z,n} &= \text{LN}(\boldsymbol{G}_{g_z} g_{z,n} + b_{g_z}) + z_{t_n} \\ \text{LS4}_{\text{gen}}(x_{[t_0,t_{n-1}]}, z_{[t_0,t_n]}, \psi) &= (\hat{g}_{x,n}, \hat{g}_{z,n}) \end{aligned} \tag{12}$$

where ψ denotes all parameters inside the block. Note that the generative block gives two streams of outputs each having the same ResNet-like structure as in the prior model, and the output of our generative block can be used as inputs for the next stack. We then define the final mean value $\mu_{x,n}$ as the result of a stack of *LS4 generative blocks*. The initial condition for generation is given as $x_{t_0} \sim \mathcal{N}(\mu_{x,0}(z_0, \theta), \sigma_x)$ where $\mu_{x,0}$ exactly follows our formulation while taking only z_{t_0} as input. The subsequent x_{t_n}'s are generated autoregressively. We specify our architecture in Appendix C and use θ to denote the union of all trainable parameters.

4.3. Inference model

The latent variable model up to time t_n has intractable posterior $p_\theta(z_{\leq t_n} \mid x_{\leq t_n})$. Therefore, we approximate this distribution with $q_\phi(z_{\leq t_n} \mid x_{\leq t_n})$ using variational inference.

We parameterize the inference distribution at time t_n to depend only on the observed path $x_{\leq t_n}$:

$$q_\phi(z_t \mid x_{\leq t_n}) = \mathcal{N}(\hat{\mu}_{z,t_n}(x_{\leq t_n}, \phi), \hat{\sigma}^2_{z,t_n}(x_{\leq t_n}, \phi)) \tag{13}$$

This choice of dependency is as noted in our objective (Equation 5). By having each z_t explicitly depending on $x_{\leq t_n}$ only, we obviate the need for explicit recurrence to obtain z_{t_n}. We can then leverage the fast convolution operation to obtain all z_t in parallel, thus achieving fast inference time, in contrast to the autoregressive nature of the prior and generative model.

LS4 inference block. The inference block is defined as

$$\begin{aligned} \hat{y}_{z,n} &= \text{GELU}(\boldsymbol{C}_{\hat{y}_z} H_{\beta_5}(x_{[t_0,t_n]}, 0, \mathbf{0}, t_{n-1}) + \boldsymbol{D}_{\hat{y}_z} x_{t_n}) \\ \text{LS4}_{\text{inf}}(x_{[t_0,t_n]}, \psi) &= \text{LN}(\boldsymbol{G}_{\hat{y}_z} \hat{y}_{z,n} + b_{\hat{y}_z}) + x_{t_n} \end{aligned} \tag{14}$$

Notice that input x is fully present in $[t_0, t_n]$ unlike in the generative model. Similar to the prior counterparts, $\hat{\mu}_{z,t}$ and $\hat{\sigma}_{z,t}$ are obtained by first feeding x_t's into a stack of inference blocks where the final block branches out to separately model the mean and variance. Due to the convolutional nature of our inference model, the training and inference can be done very efficiently, as will be demonstrated in the next and the experiment section.

4.4. LS4: Properties and Practice

We highlight some properties of LS4. In particular, we compare in the following proposition the expressive power of our generative model against structured state space models.

Proposition 4.1. *(LS4 subsumes S4.) Given any autoregressive model $r(x)$ with conditionals $r(x_n|x_{<n})$ parameterized via deep S4 models, there exists a choice of θ, λ, ϕ such that $p_{\theta,\lambda}(x) = r(x)$ and $p_{\theta,\lambda}(z|x) = q_\phi(z|x)$, i.e. the variational lower bound (ELBO) is tight.*

A proof sketch is provided in Appendix B. This result shows that LS4 subsumes autoregressive generative models based on vanilla S4 (Gu et al., 2021), given that the architecture between SSM layers is the same. Crucially, with the assumption that we are able to globally optimize the ELBO training objective, LS4 will fit the data at least as well as vanilla S4.

Scaling to arbitrary feature dimensions. So far we have assumed the input and latent signals are real numbers. The approach can be scaled to arbitrary dimensions of inputs and latents by constructing LS4 layers for each dimension which are input into a mixing linear layer. We call such parallelized SSMs *heads* and provide a pseudo-code in Appendix C.

Proposition 4.2. *(Efficiency.) For a SSM with H heads, an observation sequence of length L and hidden dimension N can be calculated in $\mathcal{O}(H(L+N)\log(L+N))$ time and $\mathcal{O}(H(L+N))$ space.*

We provide proof in Appendix B. Note that our model is much more efficient in both time and space than RNN/ODE-based methods (which requires $\mathcal{O}(N^2L)$ in time and $\mathcal{O}(NL)$ in space as discussed in Section 3.1). To demonstrate the computation efficiency, we additionally provide below pseudo-code for a single LS4 prior layer 8. The other blocks can be similarly constructed.

```
def LS4_prior_layer(z,  A, B, C, F, h_0):
    # z: (B, L, 1)
    K = C @ materialize_kernel(z, A, B,
        h_0) # O((L+N)log(L+N)) time
    CH = fft_conv(K, z)
           # O(LlogL) time and O(L) space
    y = gelu(CH + F * z)
    return y
```

Note that in practice, $\boldsymbol{A}$ is HiPPO initialized (Gu et al., 2020) and the materialized kernel includes $\boldsymbol{C}$ so that the

convolution is computed directly in the projected space, bypassing materializing the high-dimensional hidden states.

Parametrizing the initial conditions for generation. In the previous sections we mentioned that generation starts by sampling with learnable parameters $\mu_{\cdot,0}$ and $\sigma_{\cdot,0}$. These parameters can be instead given as the output from the same networks that produce each $\mu_{\cdot,<0}$ and $\sigma_{\cdot,<0}$ with input as either a learnable parameter or simply the zero vector.

5. Experiments

In this section, we verify the modeling capability of LS4 empirically. There are three main questions we seek to answer: (1) How effective is LS4 in modeling stiff sequence data? (2) How expressive is LS4 in scaling to real time-series with a variety of temporal dynamics? (3) How efficient in training and inference is LS4 in terms of wall-clock time?

5.1. Learning to generate data from stiff systems

Modeling data generated by dynamics with widely separated time scales has been proven to be particularly challenging for vanilla ODE-based approaches which make use of standard explicit solvers for inference and gradient calculation. (Kim et al., 2021) showed that as the learned dynamics *stiffen* up to track data paths, the ODE numerics start to catastrophically fail; the inference cost raises drastically and the gradient estimation process becomes ill–conditioned. These issues can be mitigated by employing implicit ODE solvers or *ad-hoc* rescalings of the learned vector field (see (Kim et al., 2021) for further details).

In turn, state–space models do not suffer from stiffness of dynamics as the numerical methods are sidestepped in favor of an exact evaluation of the convolution operator. We hereby show that LS4 is able to model data generated by a prototype stiff system.

FLAME problem We consider a simple model of flame growth (FLAME) (Wanner & Hairer, 1996), which has been extensively studied as a representative of highly stiff systems:

$$\frac{d}{dt}x_t = x_t^2 - x_t^p$$

where $p \in \{3, 4, \dots, 10\}$. For each p, 1000 trajectories are generated for $t \in [0, 1000]$ with unit increment.

Generation. In Figure 1a, we show the mean trajectories and the distribution at each time step and that our samples closely match the ground-truth data. The Latent ODE (Rubanova et al., 2019) instead fails to do so and produces non–stiff samples drastically different from the target.

Marginal Distribution. We plot the marginal distribution of the real data and the generated data from both our model and Latent ODE. Since the stiff transitions are mostly distributed before 10% of total steps, we visualize the marginal histograms at 4 time steps equally spaced between the 0.5% and 10% steps in log scale (see Figure 1b). We observe that the empirical histogram matches the ground truth distribution significantly better than what is produced by Latent ODEs, as also qualitatively visible from the samples in (a).

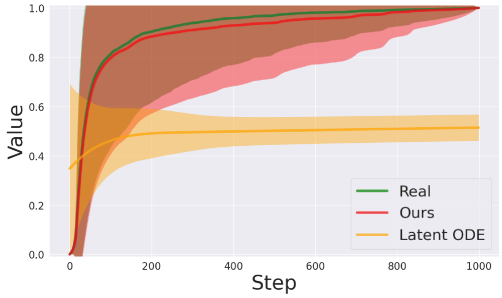

(a) Generation of the stiff system.

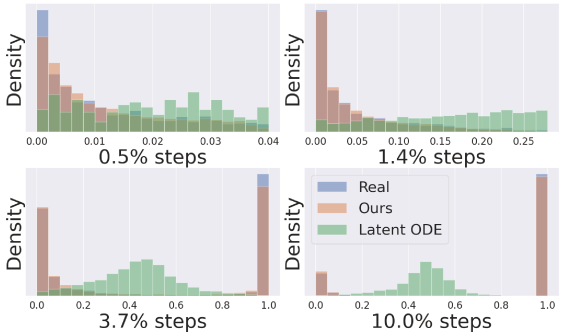

(b) Marginal histograms at steps equally spaced between the 0.5% and 10% steps in log scale.

5.2. Generation with Real Time-Series Datasets

We investigate the generative capability of LS4 on real time-series data. We show that our model is capable of fitting a wide variety of time-series data with significantly different temporal dynamics. We leave implementation details to Appendix D.1.

Data. We use Monash Time Series Repository (Godahewa et al., 2021), a comprehensive benchmark containing 30 time-series datasets collected in the real world, and we choose FRED-MD, NN5 Daily, Temperature Rain, and Solar Weekly as our target datasets. We select these datasets based on average 1-lag autocorrelation metric, which measures 1-step correlation in time, to demonstrate a variety of temporal dynamics. The selected datasets have 1-lag ranging from 0.38 to 0.98, and this wide range indicates the variety of temporal dynamics that makes generative learning a challenging task. A sample from each dataset can be visualized in Figure 2.

Metrics. We propose 3 different metrics for measuring generation performance, namely *Marginal*, *Classification*, and *Prediction* scores. *Marginal* scores calculate the absolute

Data	Metric	RNN-VAE	GP-VAE	ODE^{2}VAE	Latent ODE	TimeGAN	SDEGAN	SaShiMi	**LS4 (Ours)**
FRED-MD	Marginal ↓	0.132	0.152	0.122	0.0416	0.0813	0.0841	0.0482	**0.0221**
	Class. ↑	0.0362	0.0158	0.0282	0.327	0.0294	0.501	0.00119	**0.544**
	Prediction ↓	1.47	2.05	0.567	**0.0132**	0.0575	0.677	0.232	0.0373
NN5 Daily	Marginal ↓	0.137	0.117	0.211	0.107	0.0396	0.0852	0.0199	**0.00671**
	Class. ↑	0.000339	0.00246	0.00102	0.000381	0.00160	0.0852	0.0446	**0.636**
	Prediction ↓	0.967	1.169	1.19	1.04	1.34	1.01	0.849	**0.241**
Temp Rain	Marginal ↓	0.0174	0.183	1.831	**0.0106**	0.498	0.990	0.758	0.0834
	Class. ↑	0.00000212	0.0000123	0.0000319	0.0000419	0.00271	0.0169	0.0000167	**0.976**
	Prediction ↓	159	2.305	1.133	145	1.96	2.46	2.12	**0.521**
Solar Weekly	Marginal ↓	0.0903	0.308	0.153	0.0853	0.0496	0.147	0.173	**0.0459**
	Class. ↑	0.0524	0.000731	0.0998	0.0521	0.6489	0.591	0.00102	**0.683**
	Prediction ↓	1.25	1.47	0.761	0.973	0.237	0.976	0.578	**0.141**

Table 1: Generation results on FRED-MD, NN5 Daily, Temperature Rain, and Solar Weekly.

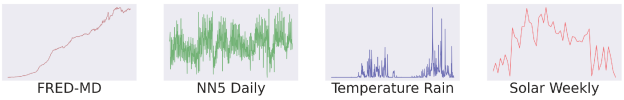

Figure 2: Monash data. The selected datasets exhibit a variety of temporal dynamics ranging from relatively smooth to stiff transitions.

difference between empirical probability density functions of two distributions – the lower the better (Ni et al., 2020). Following Kidger et al. (2021), we define *Classification* scores as using a sequence model to classify whether a sample is real or generated and use its cross-entropy loss as a proxy for generation quality – the higher the less distinguishable the samples, thus better the generation. Similarly, *Prediction* scores use a train-on-synthetic-test-on-real seq2seq model to predict k steps into the future – the lower the more predictable, thus better the generation. We use a 1-layer S4 (Gu et al., 2021) for both Classification and Prediction scores (see Appendix D.1 for more details). We will discuss the necessity of all 3 metrics in the following discussion section.

We compare our model with several time-series generative models, namely the VAE-based methods such as RNN-VAE (Rubanova et al., 2019), GP-VAE (Fortuin et al., 2020), ODE^{2}VAE (Yildiz et al., 2019), Latent ODE (Rubanova et al., 2019), GAN-based methods such as TimeGAN (Yoon et al., 2019) and SDE GAN (Kidger et al., 2021), and SaShiMi (Goel et al., 2022). Note that SaShiMi in this case is equivalent to S4 (Gu et al., 2021) as an autoregressive model with no latent variables, and suits as our closest baseline. To modify SaShiMi for general time-series, we modify its output to follow Gaussian probability with fixed variance instead of discrete tokens as in audio. We show quantitative results in Table 1.

Our model significantly outperforms the baselines on all datasets. We note that baseline models have a hard time modeling NN5 Daily and Temperature Rain where the transition dynamics are stiff. For Temperature Rain where most data points lie around x-axis with sharp spikes throughout, latent ODE generates mostly closely to the x-axis, thus achieving lower marginal scores, but its generation is easily distinguishable from data, thus making it a less favorable generative model. We demonstrate that Marginal scores alone are an insufficient metric for generation quality. SaShiMi, an autoregressive model based on S4, does not perform as well on time series generation in the tasks considered. We further discuss the reason in Appendix D.1.

5.3. Interpolation & Extrapolation

We also show that our model is expressive enough to fit to irregularly-sampled data and performs favorably in terms of interpolation and extrapolation. Interpolation refers to the task of predicting missing data given a subset of a sequence while extrapolation refers to the task that data is separated into 2 segments each with half the length of the full sequence, and one predicts the latter segment given the former.

Data. Following Rubanova et al. (2019); Schirmer et al. (2022), we use USHCN and Physionet as our datasets of choice. The United States Historical Climatology Network (USHCN) (Menne et al., 2015) is a climate dataset containing daily measurements form 1,218 weather stations across the US for precipitation, snowfall, snow depth, minimum and maximum temperature. Physionet (Silva et al., 2012) is a dataset containing health measurements of 41 signals from 8,000 ICU patients in their first 48 hours. We follow preprocessing steps of Schirmer et al. (2022) for training and testing.

Metrics. We use mean squared error (MSE) and continuous ranked probability score (CRPS) to evaluate both interpolation and extrapolation. MSE determines the absolute prediction error while CRPS measures the difference of output cumulative distributions (CDF) against ground-truth. For a point observation, the CDF is assumed to be a step function.

We compare our model with RNN (Rumelhart et al., 1985),

Metric	Task	Data	RNN	RNN-VAE	ODE-RNN	GRU-D	Latent ODE	CRU	**LS4 (Ours)**
MSE ($\times 10^{-3}$) $\downarrow$	Interp.	Physionet	2.918	5.930	2.234	3.325	8.341	1.82	**0.6287**
		USHCN	4.322	7.561	2.473	3.395	6.859	0.16	**0.0594**
	Extrap.	Physionet	3.406	3.064	**3.014**	3.120	4.212	6.29	4.942
		USHCN	9.474	9.083	9.045	8.964	8.959	12.73	**2.975**
CRPS ($\times 10^{-2}$) $\downarrow$	Interp.	Physionet	2.09	5.59	2.40	2.71	6.16	-	**1.25**
		USHCN	3.33	4.68	3.18	4.69	4.68	-	**0.438**
	Extrap.	Physionet	3.30	2.17	**2.16**	13.9	2.43	-	2.36
		USHCN	72.1	5.01	5.09	5.01	5.04	-	**2.76**

Table 2: Interpolation and extrapolation MSE ($\times 10^{-3}$) scores and CRPS ($\times 10^{-2}$) scores. Lower scores are better.

RNN-VAE (Chung et al., 2014; Rubanova et al., 2019), ODE-RNN (Rubanova et al., 2019), GRU-D (Rubanova et al., 2019), Latent ODE (Chen et al., 2018; Rubanova et al., 2019), and CRU[2](Schirmer et al., 2022). Results are shown in Table 2.

We observe that our model outperforms previous continuous-time methods. Our model performs less well on extrapolation for Physionet compared to ODE-RNN and latent ODE and we postulate that this is due to the high variability granted by our latent space. Since new latent variables are generated as we extrapolate, our model generates paths that are more flexible (hence less predictable) than those of Latent ODE, which instead uses a single latent variable to encode an entire path. We also examine LS4's ability to perform probabilistic forecasting with CRPS. Notice that MSE and CRPS are correlated. This is due to the output probability being parameterized by Gaussian with fixed variance for all models, such that the difference between the Gaussian and step CDF is correlated with the difference between their mean. We additional observe that our model achieves ELBO of -669.0 and -250.2 on Physionet interpolation and extrapolation tasks respectively. These bounds are much tighter lower bounds than other VAE-based methods, *i.e.* RNN-VAE, which reports -412.8 and -220.2, and latent ODE, which reports -410.3 and -168.5. We leave additional ELBO comparisons in Appendix D.

5.4. Runtime

We additionally verify the computational efficiency of our model for both training and inference. We do so by training and inferring on synthetic data with controlled lengths specified below.

Data. We create a set of synthetic datasets with lengths $\{80, 320, 1280, 5120, 20480\}$ to investigate scaling of training/inference time with respect to sequence length. Training is done with 100 iterations through the synthetic data, and inference is performed given one batch of synthetic data (see Appendix D.3).

Metrics. We use wall-clock runtime measured in milliseconds.

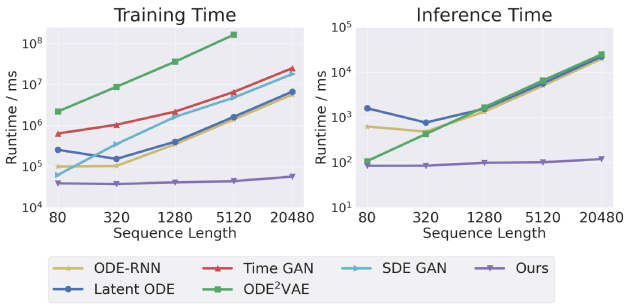

Figure 3: Runtime comparison. The y-axis shows run-time (**ms**) of each setting in log scale. Our runtime stays consistently lower across all sequence lengths investigated.

Figure 3 shows model runtime in log scale. ODE^{2}VAE fails to finish training on the last sequence length within a reasonable time frame, so we omit its plot of the last data point. Our model performs consistently and significantly lower than baselines, which are observed to scale linearly with input lengths, and is $\times 100$ faster than baselines in both training and inference on 20480 length.

6. Conclusion

We introduce LS4, a powerful generative model with latent space evolution following a state space ODE. Our model is built with a deep stack of LS4 prior/generative/inference blocks, which are trained via standard sequence VAE objectives. We also show that under specific choices of model parameters, LS4 subsumes autoregressive S4 models. Experimentally, we demonstrate the modeling power of LS4 on datasets with a wide variety of temporal dynamics and show significant improvement in generation/interpolation/extrapolation quality. In addition, our model shows $\times 100$ speed-up in training and inference time on long sequences. LS4 demonstrates improved expressivity and computational ef-

[2]Numbers are taken from the original paper. We keep the significant digits unchanged.

ficiency, and we believe that it has a further role to play in modeling general time-series sequences.

7. Acknowledgement

This research was supported in part by NSF(#1651565), ARO (W911NF-21-1-0125), ONR (N00014-23-1-2159), CZ Biohub, HAI.

References

Bayer, J. and Osendorfer, C. Learning stochastic recurrent networks. *arXiv preprint arXiv:1411.7610*, 2014.

Brooks, T., Hellsten, J., Aittala, M., Wang, T.-C., Aila, T., Lehtinen, J., Liu, M.-Y., Efros, A. A., and Karras, T. Generating long videos of dynamic scenes. *arXiv preprint arXiv:2206.03429*, 2022.

Brown, T., Mann, B., Ryder, N., Subbiah, M., Kaplan, J. D., Dhariwal, P., Neelakantan, A., Shyam, P., Sastry, G., Askell, A., et al. Language models are few-shot learners. *Advances in neural information processing systems*, 33: 1877–1901, 2020.

Burda, Y., Grosse, R., and Salakhutdinov, R. Importance weighted autoencoders. *arXiv preprint arXiv:1509.00519*, 2015.

Chen, C.-T. *Linear system theory and design*. Saunders college publishing, 1984.

Chen, R. T., Rubanova, Y., Bettencourt, J., and Duvenaud, D. K. Neural ordinary differential equations. *Advances in neural information processing systems*, 31, 2018.

Chilkuri, N. R. and Eliasmith, C. Parallelizing legendre memory unit training. In *International Conference on Machine Learning*, pp. 1898–1907. PMLR, 2021.

Chung, J., Gulcehre, C., Cho, K., and Bengio, Y. Empirical evaluation of gated recurrent neural networks on sequence modeling. *arXiv preprint arXiv:1412.3555*, 2014.

Chung, J., Kastner, K., Dinh, L., Goel, K., Courville, A. C., and Bengio, Y. A recurrent latent variable model for sequential data. *Advances in neural information processing systems*, 28, 2015.

de Bézenac, E., Rangapuram, S. S., Benidis, K., Bohlke-Schneider, M., Kurle, R., Stella, L., Hasson, H., Gallinari, P., and Januschowski, T. Normalizing kalman filters for multivariate time series analysis. *Advances in Neural Information Processing Systems*, 33:2995–3007, 2020.

De Brouwer, E., Simm, J., Arany, A., and Moreau, Y. Gru-ode-bayes: Continuous modeling of sporadically-observed time series. *Advances in neural information processing systems*, 32, 2019.

Deng, R., Chang, B., Brubaker, M. A., Mori, G., and Lehrmann, A. Modeling continuous stochastic processes with dynamic normalizing flows. *Advances in Neural Information Processing Systems*, 33:7805–7815, 2020.

Fabius, O. and Van Amersfoort, J. R. Variational recurrent auto-encoders. *arXiv preprint arXiv:1412.6581*, 2014.

Fortuin, V., Baranchuk, D., Rätsch, G., and Mandt, S. Gp-vae: Deep probabilistic time series imputation. In *International conference on artificial intelligence and statistics*, pp. 1651–1661. PMLR, 2020.

Franceschi, J.-Y., Delasalles, E., Chen, M., Lamprier, S., and Gallinari, P. Stochastic latent residual video prediction. In *International Conference on Machine Learning*, pp. 3233–3246. PMLR, 2020.

Godahewa, R., Bergmeir, C., Webb, G. I., Hyndman, R. J., and Montero-Manso, P. Monash time series forecasting archive. In *Neural Information Processing Systems Track on Datasets and Benchmarks*, 2021.

Goel, K., Gu, A., Donahue, C., and Ré, C. It's raw! audio generation with state-space models. *arXiv preprint arXiv:2202.09729*, 2022.

Gu, A., Dao, T., Ermon, S., Rudra, A., and Ré, C. Hippo: Recurrent memory with optimal polynomial projections. *Advances in Neural Information Processing Systems*, 33: 1474–1487, 2020.

Gu, A., Goel, K., and Ré, C. Efficiently modeling long sequences with structured state spaces. *arXiv preprint arXiv:2111.00396*, 2021.

Gu, A., Gupta, A., Goel, K., and Ré, C. On the parameterization and initialization of diagonal state space models. *arXiv preprint arXiv:2206.11893*, 2022.

Hersbach, H., Bell, B., Berrisford, P., Hirahara, S., Horányi, A., Muñoz-Sabater, J., Nicolas, J., Peubey, C., Radu, R., Schepers, D., et al. The era5 global reanalysis. *Quarterly Journal of the Royal Meteorological Society*, 146(730): 1999–2049, 2020.

Ho, J., Jain, A., and Abbeel, P. Denoising diffusion probabilistic models. *Advances in Neural Information Processing Systems*, 33:6840–6851, 2020.

Hochreiter, S. The vanishing gradient problem during learning recurrent neural nets and problem solutions. *International Journal of Uncertainty, Fuzziness and Knowledge-Based Systems*, 6(02):107–116, 1998.

Kidger, P., Morrill, J., Foster, J., and Lyons, T. Neural controlled differential equations for irregular time series. *Advances in Neural Information Processing Systems*, 33: 6696–6707, 2020.

Kidger, P., Foster, J., Li, X., and Lyons, T. J. Neural sdes as infinite-dimensional gans. In *International Conference on Machine Learning*, pp. 5453–5463. PMLR, 2021.

Kim, S., Ji, W., Deng, S., Ma, Y., and Rackauckas, C. Stiff neural ordinary differential equations. *Chaos: An Interdisciplinary Journal of Nonlinear Science*, 31(9):093122, 2021.

Kingma, D. P. and Welling, M. Auto-encoding variational bayes. *arXiv preprint arXiv:1312.6114*, 2013.

Li, X., Wong, T.-K. L., Chen, R. T., and Duvenaud, D. Scalable gradients for stochastic differential equations. In *International Conference on Artificial Intelligence and Statistics*, pp. 3870–3882. PMLR, 2020.

Massaroli, S., Poli, M., Park, J., Yamashita, A., and Asama, H. Dissecting neural odes. *Advances in Neural Information Processing Systems*, 33:3952–3963, 2020.

Massaroli, S., Poli, M., Sonoda, S., Suzuki, T., Park, J., Yamashita, A., and Asama, H. Differentiable multiple shooting layers. *Advances in Neural Information Processing Systems*, 34:16532–16544, 2021.

Menne, M., Williams Jr, C., and Vose, R. Long-term daily climate records from stations across the contiguous united states, 2015.

Ni, H., Szpruch, L., Wiese, M., Liao, S., and Xiao, B. Conditional sig-wasserstein gans for time series generation. *arXiv preprint arXiv:2006.05421*, 2020.

Niesen, J. and Hall, T. *On the global error of discretization methods for ordinary differential equations*. PhD thesis, Citeseer, 2004.

Oord, A. v. d., Dieleman, S., Zen, H., Simonyan, K., Vinyals, O., Graves, A., Kalchbrenner, N., Senior, A., and Kavukcuoglu, K. Wavenet: A generative model for raw audio. *arXiv preprint arXiv:1609.03499*, 2016.

Oppenheim, A. V. *Discrete-time signal processing*. Pearson Education India, 1999.

Oppenheim, A. V. and Schafer, R. W. Digital signal processing(book). *Research supported by the Massachusetts Institute of Technology, Bell Telephone Laboratories, and Guggenheim Foundation. Englewood Cliffs, N. J., Prentice-Hall, Inc., 1975. 598 p*, 1975.

Peng, C.-K., Havlin, S., Stanley, H. E., and Goldberger, A. L. Quantification of scaling exponents and crossover phenomena in nonstationary heartbeat time series. *Chaos: an interdisciplinary journal of nonlinear science*, 5(1): 82–87, 1995.

Poli, M., Park, J., and Ilievski, I. Wattnet: learning to trade fx via hierarchical spatio-temporal representation of highly multivariate time series. *arXiv preprint arXiv:1909.10801*, 2019.

Rasul, K., Seward, C., Schuster, I., and Vollgraf, R. Autoregressive denoising diffusion models for multivariate probabilistic time series forecasting. In *International Conference on Machine Learning*, pp. 8857–8868. PMLR, 2021.

Romero, D. W., Kuzina, A., Bekkers, E. J., Tomczak, J. M., and Hoogendoorn, M. Ckconv: Continuous kernel convolution for sequential data. *arXiv preprint arXiv:2102.02611*, 2021.

Rubanova, Y., Chen, R. T., and Duvenaud, D. K. Latent ordinary differential equations for irregularly-sampled time series. *Advances in neural information processing systems*, 32, 2019.

Rumelhart, D. E., Hinton, G. E., and Williams, R. J. Learning internal representations by error propagation. Technical report, California Univ San Diego La Jolla Inst for Cognitive Science, 1985.

Schirmer, M., Eltayeb, M., Lessmann, S., and Rudolph, M. Modeling irregular time series with continuous recurrent units. In *International Conference on Machine Learning*, pp. 19388–19405. PMLR, 2022.

Shampine, L. F. and Thompson, S. Stiff systems. *Scholarpedia*, 2(3):2855, 2007.

Silva, I., Moody, G., Scott, D. J., Celi, L. A., and Mark, R. G. Predicting in-hospital mortality of icu patients: The physionet/computing in cardiology challenge 2012. In *2012 Computing in Cardiology*, pp. 245–248. IEEE, 2012.

Sohl-Dickstein, J., Weiss, E., Maheswaranathan, N., and Ganguli, S. Deep unsupervised learning using nonequilibrium thermodynamics. In *ICML*, 2015.

Song, Y. and Ermon, S. Generative modeling by estimating gradients of the data distribution. *NeurIPS*, 32, 2019.

Song, Y., Sohl-Dickstein, J., Kingma, D. P., Kumar, A., Ermon, S., and Poole, B. Score-based generative modeling through stochastic differential equations. *arXiv preprint arXiv:2011.13456*, 2020.

Tashiro, Y., Song, J., Song, Y., and Ermon, S. Csdi: Conditional score-based diffusion models for probabilistic time series imputation. *Advances in Neural Information Processing Systems*, 34:24804–24816, 2021.

Wanner, G. and Hairer, E. *Solving ordinary differential equations II*, volume 375. Springer Berlin Heidelberg New York, 1996.

Yildiz, C., Heinonen, M., and Lahdesmaki, H. Ode2vae: Deep generative second order odes with bayesian neural networks. *Advances in Neural Information Processing Systems*, 32, 2019.

Yoon, J., Jarrett, D., and Van der Schaar, M. Time-series generative adversarial networks. *Advances in neural information processing systems*, 32, 2019.

Yu, L., Zhang, W., Wang, J., and Yu, Y. Seqgan: Sequence generative adversarial nets with policy gradient. In *Proceedings of the AAAI conference on artificial intelligence*, volume 31, 2017.

Yu, S., Tack, J., Mo, S., Kim, H., Kim, J., Ha, J.-W., and Shin, J. Generating videos with dynamics-aware implicit generative adversarial networks. *arXiv preprint arXiv:2202.10571*, 2022.

Zhuang, J., Dvornek, N., Li, X., Tatikonda, S., Papademetris, X., and Duncan, J. Adaptive checkpoint adjoint method for gradient estimation in neural ode. In *International Conference on Machine Learning*, pp. 11639–11649. PMLR, 2020.

Deep Latent State Space Models for Time-Series Generation

A. Derivations

A.1. Computational Complexity of Vanilla Recurrent Representation

Assuming recurrence of the simplest form in Equation 2, fulling computing matrix multiplication $\bar{\boldsymbol{A}}\bar{h}_{t_k}$ requires $\mathcal{O}(N^2)$. Fully computing all hidden states sequentially requires $\mathcal{O}(N^2L)$. In space, saving each hidden state requires $\mathcal{O}(N)$ and in total requires $\mathcal{O}(NL)$.

B. Proof

To prove this result in Proposition 4.1, we first prove the following proposition.

Proposition B.1. *(Expressivity.) Given any deep autoregressive S4 model $r : (x_{<t_n}, t_n) \mapsto y_{t_n}$ evaluated at time t_n given input sequence $x_{<t_n}$, there exists a choice of θ such that $\mu_{x,n}(x_{<t_n}, 0, \theta) = r(x_{<t_n}, t_n)$.*

Proof sketch. Consider SSM of the form in Equation 6 as a building block to our generative model with parameter θ. We can choose $\boldsymbol{E} = \boldsymbol{F} = 0$ for all layers, which exactly reduces it to the SSM of an S4 model. Keeping all other hyperparameters (*e.g.* non-linearities, number of stacking layers) the same, the final model is exactly the same as a deep autoregressive S4 model. □

Now we give a proof sketch to Proposition 4.1,

Proposition 4.1. *(LS4 subsumes S4.) Given any autoregressive model $r(x)$ with conditionals $r(x_n|x_{<n})$ parameterized via deep S4 models, there exists a choice of θ, λ, ϕ such that $p_{\theta,\lambda}(x) = r(x)$ and $p_{\theta,\lambda}(z|x) = q_\phi(z|x)$, i.e. the variational lower bound (ELBO) is tight.*

Proof sketch. From Proposition B.1 we know that we can choose θ so that $p_\theta(x|z) = p_\theta(x) = r(x)$ for all z, i.e., choose a decoder that ignores the latent variables z and uses the same autoregressive structure over the observed variables as $r(x)$. This implies the posterior $p_{\theta,\lambda}(z|x)$ is equal to the prior $p_\lambda(z)$. We can then choose λ and ϕ so that $p_\lambda(z) = \mathcal{N}(0, I)$ and $q_\phi(z|x) = \mathcal{N}(0, I)$ for all x. □

Proposition 4.2. *(Efficiency.) For a SSM with H heads, an observation sequence of length L and hidden dimension N can be calculated in $\mathcal{O}(H(L+N)\log(L+N))$ time and $\mathcal{O}(H(L+N))$ space.*

Proof. Recall *SISO* SSM of the form

$$\begin{aligned} \frac{d}{dt}\boldsymbol{h}_t &= \boldsymbol{A}\boldsymbol{h}_t + \boldsymbol{B}x_t \\ y_t &= \boldsymbol{C}\boldsymbol{h}_t + \boldsymbol{D}x_t \end{aligned} \tag{15}$$

The calculation of $(y_{t_0}, \ldots, y_{t_L})$ involves materializing the convolution filter, which can be calculated in $\mathcal{O}((L+N)\log(L+N))$ time and $\mathcal{O}(L+N)$ space for diagonal-plus-low-rank matrices (Gu et al., 2021). Since the convolution is constant time in frequency domain, another computation cost comes from Fast Fourier Transform (FFT) and its inverse, which is $\mathcal{O}(L\log L)$ in time. The computation scales linearly with heads, Thus, a multi-input-multi-output (MIMO) SSM with H heads can be processed in $\mathcal{O}(H(L+N)\log(L+N))$ time and $\mathcal{O}(H(L+N))$ space. □

C. Architecture

We parametrize our models using a similar architecture as in Goel et al. (2022), but there is no pooling operation because for general time-series the time length is hardly divisible by a reasonable factor. Before we present the full structure, we present how a multi-channel inputs are parametrized (in the case of LS4 prior layer (8):

```
def LS4_prior_layer_multi(z, psi):
    # z: (B, L, C)
    for c in range(C):
        z[:,:,c] = LS4_prior_layer(z[:,:,c], *psi.LS4_params)
    z = linear(z) # (B, L, C)  channel-wise mixing
    return z
```

The for loop is presented for demonstration purposes. In practice, the channels can be processed in parallel.

C.1. Prior Model

We specify the parametrization of $\mu_{z,n}$ and $\sigma_{z,n}$ in pseudo-code as the outputs of the following functions

```
def prior_model(z, lambda):
    # z: (B, L, z_dim) this is for time [t_0, t_{n-1}]
    z = linear(z) # (B,L,H) encoding to H

    outputs = []
    outputs.append(z)
    for i in range(lambda.num_layers1):
        z = linear(z) #  (B, L, H) -> (B, L, 2H)
        outputs.append(z)

    for i in range(lambda.num_layers2):
        z = LS4_prior_block_multi(z, *lambda.LS4_params)
              # (B, L, H) -> (B, L, H) multi-channel SSMs
        z = ResBlock(z) # this is a general 1 layer residual block
    z = z + outputs.pop()

    for i in range(lambda.num_layers1):
        z = z + outputs.pop()
        outputs.append(z)
        z = linear(z)  #  (B, L, 2H) -> (B, L, H)
        for i in range(lambda.num_layers2):
            z = LS4_prior_block_multi(z, *lambda.LS4_params)
                # (B, L, H) -> (B, L, H) multi-channel SSMs
            z = ResBlock(z) # this is a general 1 layer residual block

        z = z + outputs.pop()
    z = layernorm(z)
    z = linear(z) # (B,L,z_dim)
    mu_z = LS4_prior_block_multi(z, *lambda.LS4_params) # (B,L,z_dim)
    sigma_z = LS4_prior_block_multi(z, *lambda.LS4_params)
                                                        # (B,L,z_dim)
    return mu_z, sigma_z
```

C.2. Generative Model

```
def prior_model(x, z, theta):
    # z: (B, L, z_dim) this is for time [t_0, t_{n-1}]
    z = linear(z) # (B,L,H) encoding to H
    x = linear(x) # (B,L,H) encoding to H

    outputs_x, outputs_z = [], []
    outputs_z.append(z)
    outputs_x.append(x)
    for i in range(lambda.num_layers1):
        z = linear(z) #  (B, L, H) -> (B, L, 2H)
        x = linear(x) #  (B, L, H) -> (B, L, 2H)
        outputs_z.append(z)
        outputs_x.append(x)

    for i in range(lambda.num_layers2):
        z, x = LS4_gen_block_multi(z, *lambda.LS4_params)
```

```
                # (B, L, H) -> (B, L, H) multi-channel SSMs
        zx = ResBlock(concat(z, x))
                # this is a general 1 layer residual block
        z, x = split(z, x)
    z = z + outputs_z.pop()
    x = x + outputs_x.pop()

    for i in range(lambda.num_layers1):
        z = z + outputs_z.pop()
        x = x + outputs_x.pop()
        outputs_z.append(z)
        outputs_x.append(z)
        z = linear(z)  #  (B, L, 2H) -> (B, L, H)
        x = linear(x)  #  (B, L, 2H) -> (B, L, H)
        for i in range(lambda.num_layers2):
            x, z = LS4_gen_block_multi(x, z, *lambda.LS4_params)
                        # (B, L, H) -> (B, L, H) multi-channel SSMs
            zx = ResBlock(concat(z, x))
                # this is a general 1 layer residual block
            z, x = split(z, x)

        z = z + outputs_z.pop()
        x = x + outputs_x.pop()
    x = layernorm(x)
    z = layernorm(z)
    x = linear(concat(x, z)) # (B,L,2H) -> (B,L,x_dim)
    return mu_x
```

In practice, we find that only using z input for the entire generative model produces better generation better than including x. We hypothesize that x presents too strong of a signal for the model to reconstruct, and so the model learns to ignore signals from z in that case.

C.3. Inference Model

```
def inference_model(x, phi):
    # x: (B, L, x_dim) this is for time [t_0, t_{n-1}]
    x = linear(x) # (B,L,H) encoding to H

    outputs = []
    outputs.append(x)
    for i in range(phi.num_layers1):
        x = linear(x) #  (B, L, H) -> (B, L, 2H)
        outputs.append(x)

    for i in range(phi.num_layers2):
        x = LS4_inf_block_multi(x, *phi.LS4_params)
                # (B, L, H) -> (B, L, H) multi-channel SSMs
        z = ResBlock(z) # this is a general 1 layer residual block
    x = x + outputs.pop()

    for i in range(phi.num_layers1):
        x = x + outputs.pop()
        outputs.append(x)
        x = linear(x)  #  (B, L, 2H) -> (B, L, H)
        for i in range(phi.num_layers2):
            x = LS4_inf_block_multi(x, *phi.LS4_params)
                    # (B, L, H) -> (B, L, H) multi-channel SSMs
            z = ResBlock(z) # this is a general 1 layer residual block

        x = x + outputs.pop()
    x = layernorm(x)
    x = linear(x) # (B,L,x_dim)
    mu_z = LS4_inf_block_multi(x, *phi.LS4_params) # (B,L,x_dim)
    sigma_z = LS4_inf_block_multi(x, *phi.LS4_params)
```

```
                                                    # (B,L,x_dim)
        return mu_z, sigma_z
```

D. Experiments

For all experiments we use AdamW optimizer with learning rate 0.001. We use batch size 64 and train for 7000 epochs for FRED-MD, NN5 Daily, and Solar Weekly, 1000 epochs for Temperature Rain, and 500 epochs for Physionet and USHCN. The datasets are split into 80% training data and 20% testing data.

D.1. MONASH Forecasting Repository

Data. For all selected MONASH data, FRED-MD, NN5 Daily, and Solar Weekly are normalized per sequence such that each trajectory is centered at its own mean and normally distributed. We make this choice from the observation that for some datasets such as NN5 Daily the min and max can vary significantly across different data points such that normalizing sequences with dataset-wise statistics makes it difficult to learn the temporal dynamics, which would be on a widely different range. For Temperature Rain we squash each sequence into $[0, 1]$. This is due to the fact that the dataset is always positive and lands mostly around x-axis with sharp spikes in between. For the former 3 datasets, we do not use output activation while for the last, we use sigmoid as our activation.

Hyperparameters. For all MONASH experiments, we use AdamW optimizer with learning rate 0.001 and no weight decay. For each of prior/generative/inference model, we use 4 stacks for each for loop in the pseudocode. For each LS4 block, we use 64 as the dimension of $\mathbf{h}_t$ and 64 SSM channels in parallel, same as used in S4 and SaShiMi. Each residual block consists of 2 linear layers with skip connection at the output level where the first linear layer has 2 times output size as the input size and the second layer squeezes it back to the input size of the residual block. We generally find 5-dimensional latent space gives better performance than 1, and so uses this setting throughout. We also employ EMA for model weights and use 0.999 as the lambda value, but we do not find this choice crucial. We also use 0.1 as the standard deviation for the observation as this gives better ELBO than other choices we experimented with such as $1, 0.5, 0.01$. For baselines, we reuse the code from official repo and follow their suggestions for training. To keep representation power similar, we use the same size for the latent space (for latent variable models) and the same output standard deviation for ELBO evaluation.

Evaluation. For generation evaluation. The classification model and the prediction model uses a linear encoder and linear decoder with a single S4 layer in between. The S4 layer uses 16 hidden state dimensions. For classification model, encoder maps data dimension to 16 hidden state dimension, and averages over the sequence output from S4 layer before feeding into decoder that outputs logit for binary classification. We use cross entropy loss. For prediction model, we use the same linear encoder and a decoder that maps 16 hidden dimension to data dimension. We predict $k = 10$ steps into the future. The evaluation models are trained using AdamW with 0.01 learning rate for 100 epochs with batch size 128. We generate samples equal to the number of testing data, which together are used to train the two models.

Additional discussion. We also briefly discuss the surprising result that SaShiMi does not perform as well on general time-series generation. We speculate that not using a quantization scheme to define discrete output conditionals, as standard in autoregressive models for e.g., audio and images, is the cause behind this drop in performance. LS4 does not requires quantization and sets best performance with a simple Gaussian conditional on the data space.

Additional comparisons. We additionally compare with two more relevant baselines (Fabius & Van Amersfoort, 2014) and (Li et al., 2020) present result in Table 3. We note that Latent SDE has an abnormally high classification score for Temperature Rain data, and demonstrate that this is when the classification score is not reliable. Upon visually examining generated results for Latent SDE (Figure 4) compared to ground-truths (Figure 7), one can observe that the variation is extremely noisy around the x-axis and that the selected classifier is not powerful enough to capture the distinction from real data due to the considerable noise that exists in both generated and real data, resulting in high classification score. Marginal and predictive scores are much worse in comparison and are more indicative of generation quality.

D.2. Physionet & USHCN

We follow the code provided by Rubanova et al. (2019) to process Physionet and follow the code provided by De Brouwer et al. (2019) for USHCN. For Physionet we do not use any activation to constrain the output space, and for USHCN, we use sigmoid activation for output.

Data	Metric	VRNN	Latent SDE	**LS4 (Ours)**
FRED-MD	Marginal ↓	0.165	0.122	**0.0221**
	Class. ↑	0.000970	**0.687**	0.544
	Prediction ↓	0.371	1.62	**0.0373**
NN5 Daily	Marginal ↓	0.151	0.125	**0.00671**
	Class. ↑	0.00176	0.601	**0.636**
	Prediction ↓	1.22	0.957	**0.241**
Temp Rain	Marginal ↓	1.20	0.999	**0.0834**
	Class. ↑	0.479	**14.534**	0.976
	Prediction ↓	0.864	1.798	**0.521**
Solar Weekly	Marginal ↓	0.297	0.234	**0.0459**
	Class. ↑	0.00164	0.764	**0.683**
	Prediction ↓	0.964	1.01	**0.141**

Table 3: Additional generation results on FRED-MD, NN5 Daily, Temperature Rain, and Solar Weekly.

Task	Data	RNN-VAE	Latent ODE	**LS4 (Ours)**	**LS4$^{\text{IWAE}}$ (Ours)**
Interp.	Physionet	-412.8	-410.3	-669.0	**-684.3**
	USHCN	-244.9	-251.0	-312.2	**-315.6**
Extrap.	Physionet	-220.2	-168.5	-250.2	**-288.7**
	USHCN	-113.3	-110.3	-194.4	**-211.8**

Table 4: ELBO comparisons with VAE-based models.

We present the variational lowerbound results in Table 4.

Hyperparameters. In general we keep the hyperparameter choices the same as in MONASH, and we describe a few differences for these 2 datasets. For USHCN, we use 10 as the dimension for latent space, same as in Rubanova et al. (2019) and we use Sigmoid as the output activation with output standard deviation 0.01. For Physionet, we use no output activation and 0.05 standard deviation, and use 20-dimensional latent space, same as in baselines.

D.3. Runtime

We test all models on a single RTX A5000 GPU. To set up the dataset, we need to fully populate the GPU for each dataset during training for our benchmarking. For sequence lengths $\{80, 320, 1280, 5120, 20480\}$, we build dataset of length $\{102400, 25600, 6400, 1600, 400\}$ each with batch size $\{1024, 256, 64, 16, 4\}$ so that for each dataset the models are trained with 100 iterations.

E. Generation Results

We present ground-truths and generations on the two hardest selected datasets, NN5 Daily and Temperature Rain because these are the hardest to model.

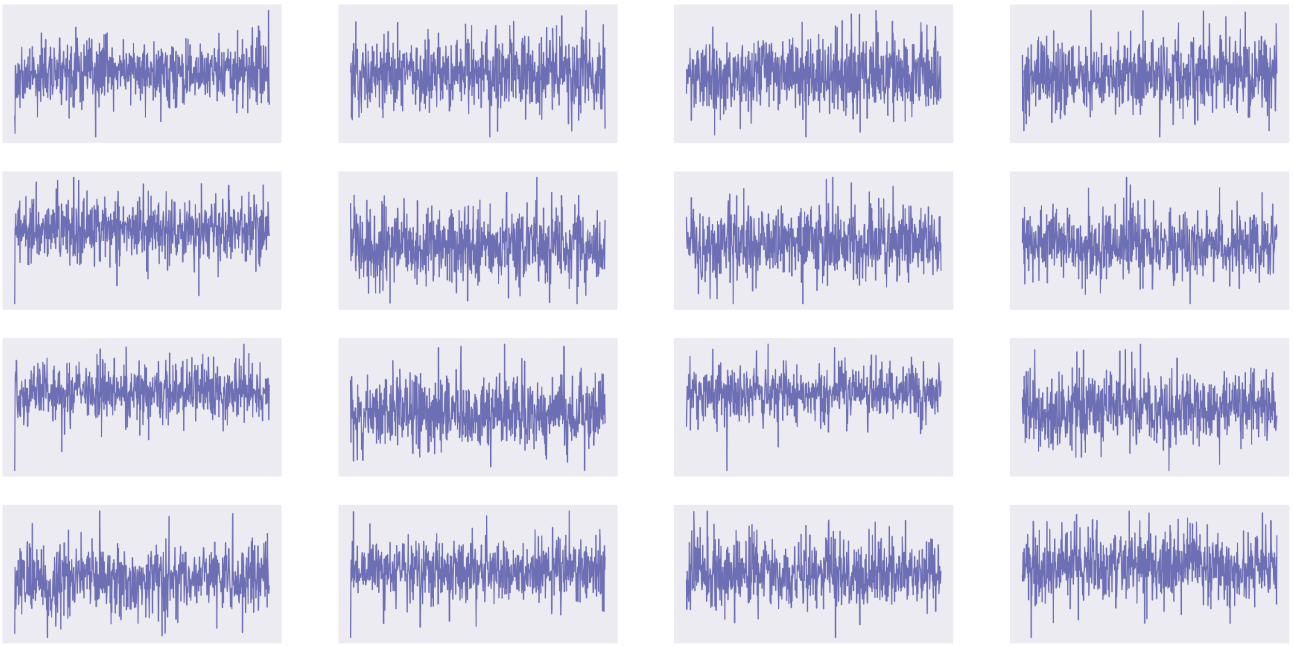

Figure 4: Latent SDE generation on Temperature Rain.

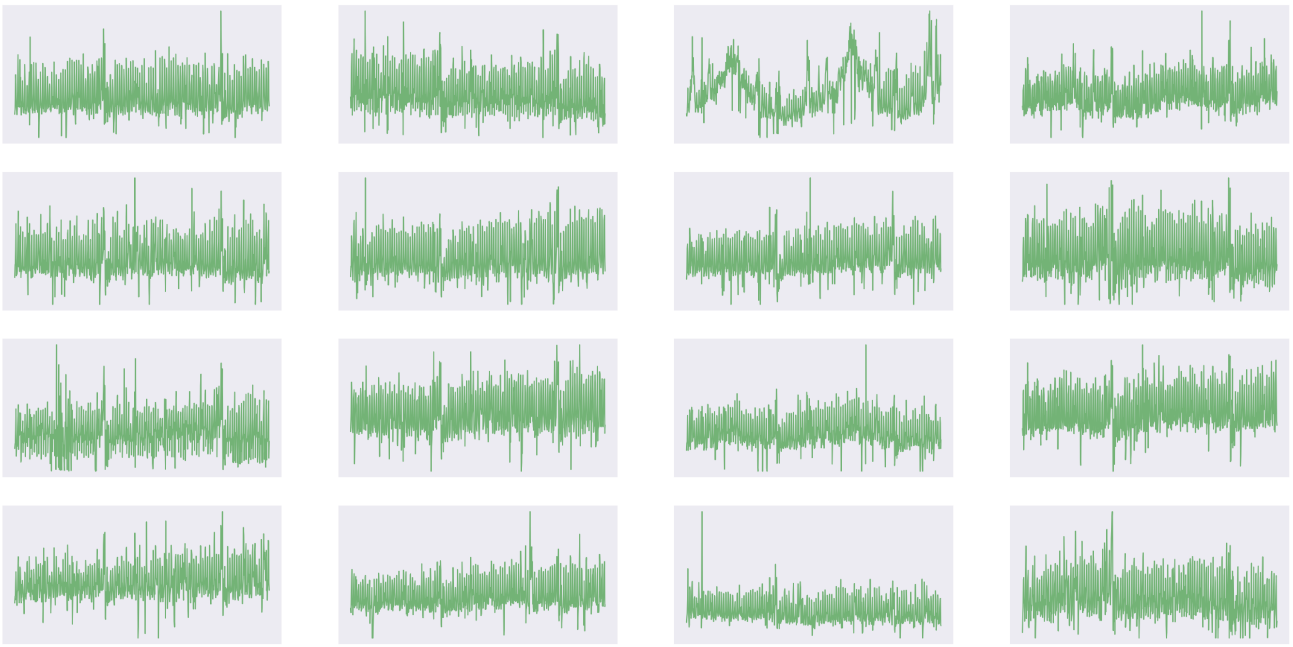

Figure 5: Normalized NN5 Daily data.

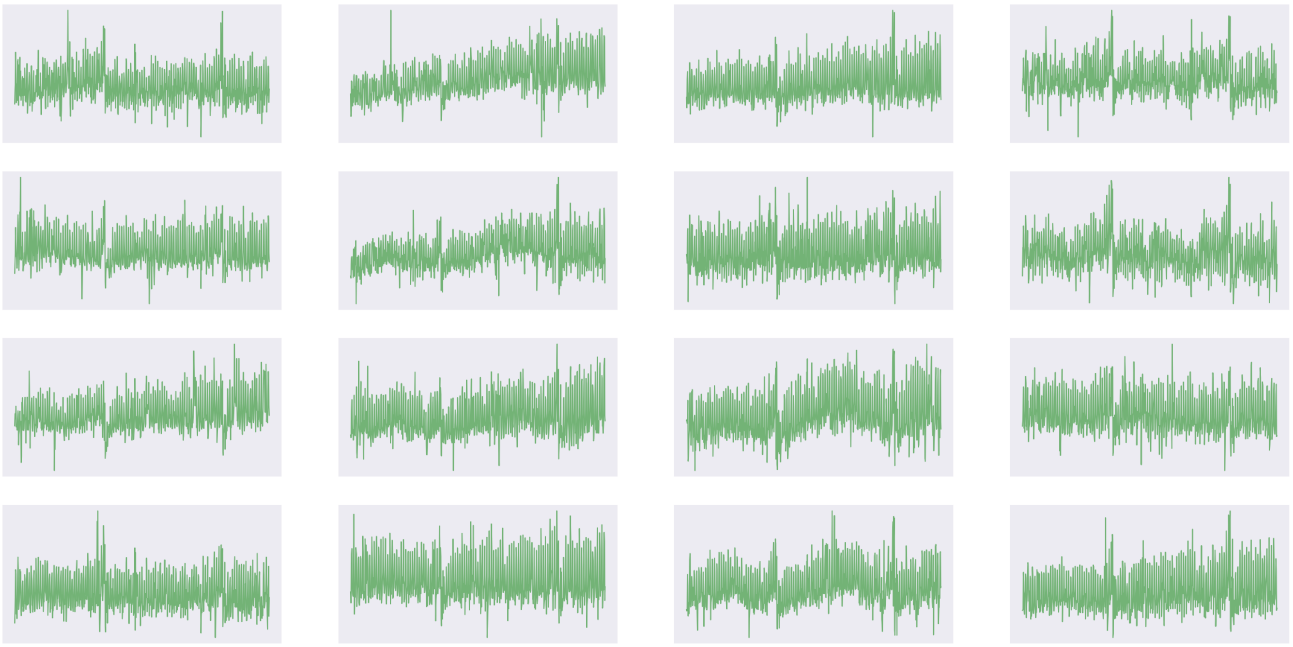

Figure 6: NN5 Daily generation.

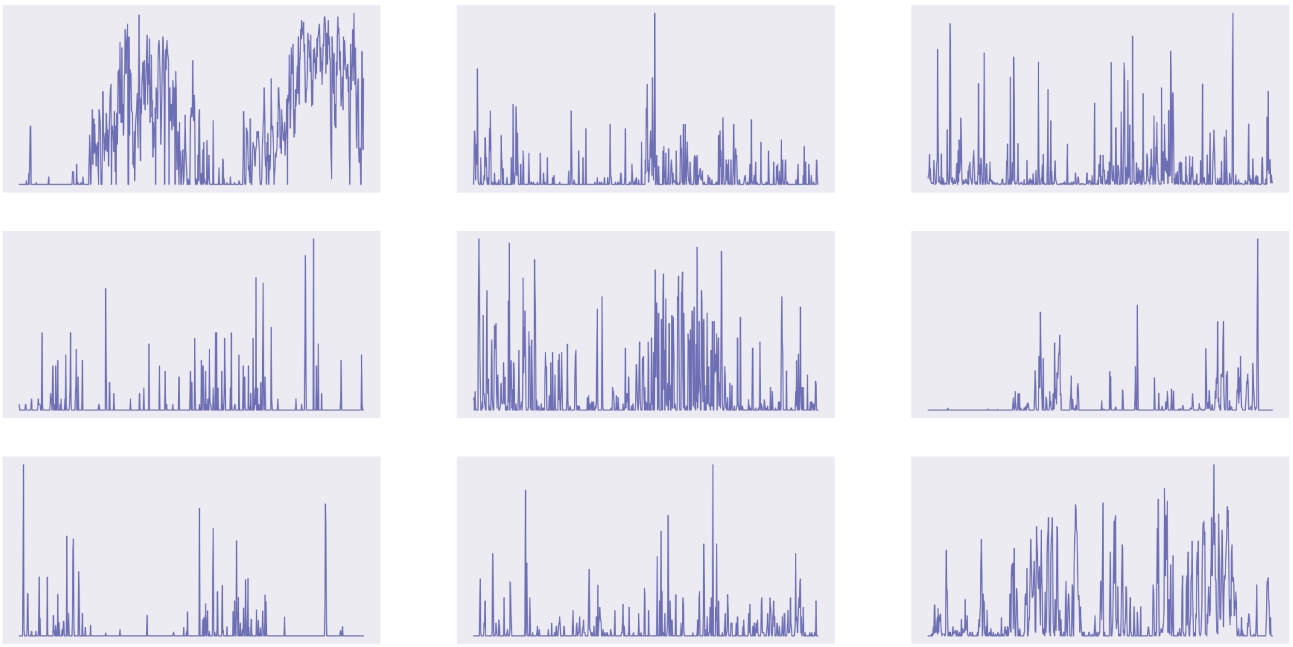

Figure 7: Normalized Temperature Rain data.

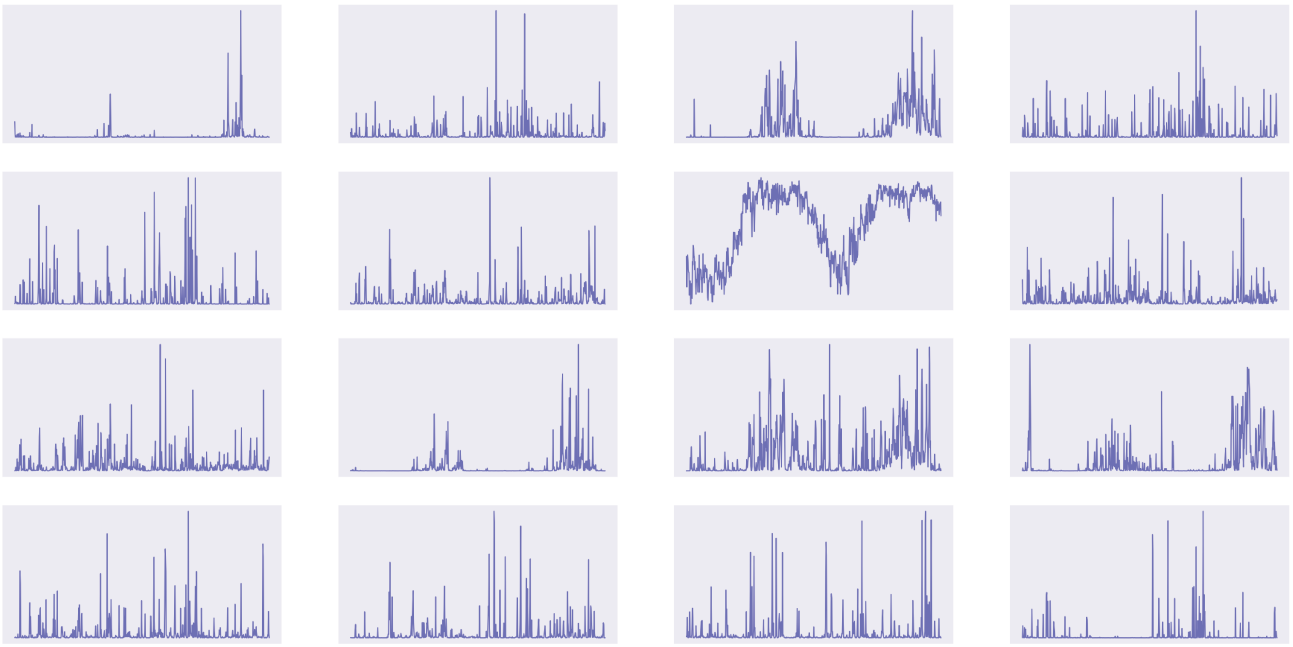

Figure 8: Temperature Rain generation.